A New Dataset and A Baseline Model for Breast Lesion Detection in Ultrasound Videos

Zhi Lin[1] *, Junhao Lin[1] *, Lei Zhu[2,3(✉)], Huazhu Fu[4],
Jing Qin[5], and Liansheng Wang[1]

[1] Department of Computer Science, School of Informatics,
Xiamen University, Xiamen, China
[2] ROAS Thrust, System Hub, The Hong Kong University of Science and
Technology (Guangzhou), Guangzhou, China
`leizhu@ust.hk`
[3] Department of Electronic and Computer Engineering, The Hong Kong University of
Science and Technology, Hong Kong SAR, China
[4] Institute of High Performance Computing, Agency for Science,
Technology and Research, Singapore
[5] School of Nursing, The Hong Kong Polytechnic University, Kowloon, Hong Kong

Abstract. Breast lesion detection in ultrasound is critical for breast cancer diagnosis. Existing methods mainly rely on individual 2D ultrasound images or combine unlabeled video and labeled 2D images to train models for breast lesion detection. In this paper, we first collect and annotate an ultrasound video dataset (188 videos) for breast lesion detection. Moreover, we propose a clip-level and video-level feature aggregated network (CVA-Net) for addressing breast lesion detection in ultrasound videos by aggregating video-level lesion classification features and clip-level temporal features. The clip-level temporal features encode local temporal information of ordered video frames and global temporal information of shuffled video frames. In our CVA-Net, an inter-video fusion module is devised to fuse local features from original video frames and global features from shuffled video frames, and an intra-video fusion module is devised to learn the temporal information among adjacent video frames. Moreover, we learn video-level features to classify the breast lesions of the original video as benign or malignant lesions to further enhance the final breast lesion detection performance in ultrasound videos. Experimental results on our annotated dataset demonstrate that our CVA-Net clearly outperforms state-of-the-art methods. The corresponding code and dataset are publicly available at `https://github.com/jhl-Det/CVA-Net`.

Keywords: Breast lesion detection in ultrasound videos · Inter-video fusion module · Intra-video fusion module · Clip/video aggregation.

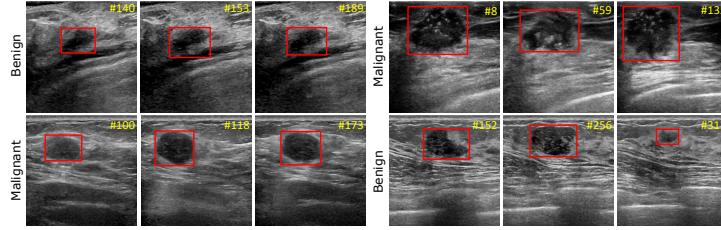* Z. Lin and J. Lin—Equal contribution.

Fig. 1. Examples of our annotated ultrasound video dataset for breast lesion detection.

1   Introduction

Breast cancer is a leading cause of death for women worldwide [16]. Currently, ultrasound imaging is the most commonly used and effective technique for breast cancer detection due to its versatility, safety, and high sensitivity [13]. Detecting breast lesions in ultrasound is often taken as an important step of computer-aided diagnosis systems to assist radiologists in the ultrasound-based breast cancer diagnosis [20,23,1]. However, accurate breast lesion detection in ultrasound videos is challenging due to blurry breast lesion boundaries, inhomogeneous distributions, changeable breast lesion sizes and positions in dynamic videos.

Existing methods [19,9,21,10,18] mainly performed the breast lesion segmentation or detection in 2D ultrasound images, or fused unlabeled videos with labeled 2D images for ultrasound video breast lesion detection. With the dominated results of convolutional neural networks on medical imaging, it is highly desirable to extend deep-learning-based breast lesion detection from the image level to video level, since the latter can leverage temporal consistency to address many in-frame ambiguities. The major obstacle for this extension is the lack of an ultrasound video dataset with appropriate annotations for breast lesion segmentation, both of which are essential for training deep models for breast lesion segmentation in ultrasound videos.

To do so, we in this work first provide a video dataset for breast lesion detection in ultrasound; see Fig. 1 for several examples of annotated videos. Then, we present a novel network for boosting breast lesion detection in ultrasound videos by aggregating video-level classification features and clip-level temporal features, which contains a local temporal feature from the input video frames and a global temporal information from shuffled video frames. The contributions of this work could be summarised as: 1) We develop a novel network to learn clip-level temporal features and video-level lesion classification features for boosting breast lesion detection in ultrasound videos. 2) We collect and annotate a video dataset (118 videos) for breast lesion detection in ultrasound videos. 3) An inter-video fusion module is devised to attentively aggregate local features from the original video frames and global features from the shuffled video frames, while an intra-video fusion module is developed to fuse temporal features encoded among adjacent video frames. 4) Experimental results on our annotated dataset

demonstrate that our network sets a new state-of-the-art performance on breast lesion detection in ultrasound videos.

2   Method

Fig. 2 shows the schematic illustration of the developed clip-level and video-level feature aggregation network (CVA-Net). The motivation behind our CVA-Net is to integrate video-level lesion classification features and clip-level features from adjacent video frames, and such clip-level features include local temporal information from the original video and global temporal information from the shuffled video. To do so, given an input ultrasound video with T frames, we first shuffle the ordered frames index sequence $\{1, \cdots, T\}$ of the input video to obtain a new index sequence, which is then used to generate a shuffled video. For a current video frame (I_k), our CVA-Net takes three neighboring images (denoted as I_k, I_{k-1}, and I_{k+1}) of the input video, and then passes I_k, I_{k-1}, and I_{k+1} into a feature extraction backbone (i.e., ResNet50 [5]) with three convolutional layers to obtain three features, which are denoted as L_k, L_{k-1}, and L_{k+1}). Apparently, L_k, L_{k-1}, and L_{k+1} contain three CNN feature maps with different spatial resolutions. Meanwhile, we take three corresponding images (denoted as S_k, S_{k-1}, and S_{k+1}) of the shuffled video, apply data augmentation techniques (e.g., horizontal flip, random crop, random pepper) on them, and pass augmented images into the feature extraction backbone to produce another three features G_k, G_{k-1}, and G_{k+1}. Afterwards, we devise an inter-video fusion module to integrate local temporal features (L_k, L_{k-1}, and L_{k+1}) from input ultrasound video, and global features (G_k, G_{k-1}, and G_{k+1}) from the shuffled video to obtain three features, which are denoted as P_k, P_{k-1}, and P_{k+1}. Then, we devise an intra-video fusion to fuse these three features P_k, P_{k-1}, and P_{k+1} to produce a new feature map Q_k, which is then passed into a classifier to predict whether the breast lesions are benign or malignant, and a bounding box predictor to produce the final breast lesion detection of the current video frame I_k.

2.1   Inter-video Fusion Module

Existing breast lesion detection in ultrasound video methods [1] extracted the temporal information encoded in ordered video frames sampled from the input video [2]. Unlike this, we devise an inter-video fusion module to utilize three frames from a shuffled video to remove the temporal order and enhance the global semantic information for detecting breast lesions. As shown in Fig. 2, our inter-video fusion module has three inter-video fusion blocks to fuse three pairs of local features and global features, which are L_k and G_k, L_{k-1} and G_{k-1}, as well as L_{k+1} and G_{k+1}, respectively. By doing so, we can fuse the local information from the input video and the global information from the shuffled video, thereby improving the video breast lesion detection.

Figure 3(a) depicts the schematic illustration of the inter-video fusion block, which integrates the local feature $L_k = (L_k^1, L_k^2, L_k^3)$ and the global feature $G_k = (G_k^1,$
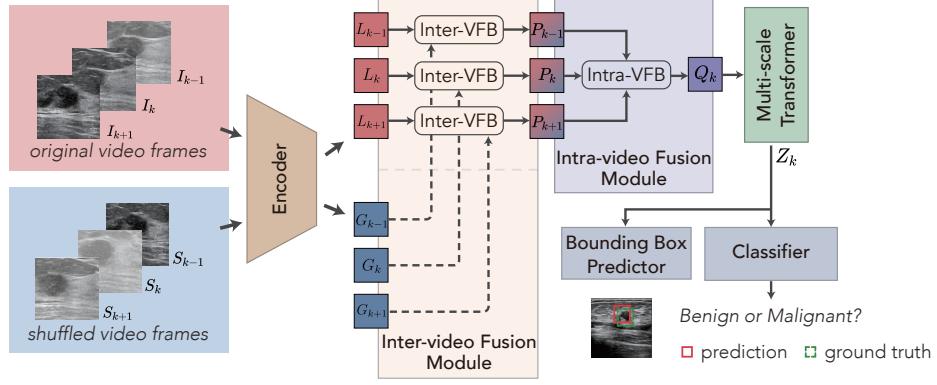
Fig. 2. Schematic illustration of our clip/video-level feature aggregation network (CVA-Net) for breast lesion detection network in ultrasound videos. "Inter-VFB" and "Intra-VFB" denotes a inter-video fusion block and a intra-video fusion block.
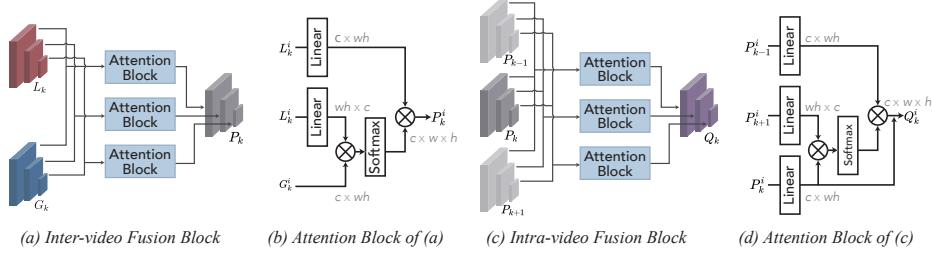

(a) Inter-video Fusion Block   (b) Attention Block of (a)   (c) Intra-video Fusion Block   (d) Attention Block of (c)

Fig. 3. Schematic illustration of the inter-video fusion module and intra-video fusion module of our network (see Figure 2).

G_k^2, G_k^3). The inter-video fusion block utilizes three attention blocks to integrate three features of L_k and G_k, and the i-th attention is for L_k^i and G_k^i (i=1,2,3); see Figure 3(b). Specifically, we first apply two different linear layers on L_k^i, reshape both of them into two $c \times wh$ matrices, and also reshape L_k^i into a $wh \times c$ matrix. Then we multiply two reshaped matrices to obtain a similarity matrix ($wh \times wh$), followed by a softmax layer. Then, we multiple the result with another reshaped matrix of L_k^i, and reshape the multiplication output to obtain the output feature H_k^i ($c \times w \times h$). Mathematically, P_k^i is computed by:

$$P_k^i = \hat{L}_k^i \times Softmax\left(\mathcal{R}(G_k^i) \times \mathcal{R}(\tilde{L}_k^i)\right) \;, \tag{1}$$

where $\mathcal{R}$ denotes a reshape operation. $\tilde{L}_k^i$ and $\hat{L}_k^i$ represents the obtained features via utilizing two different linear layers on the input feature L_k^i.

2.2   Intra-video Fusion Module

Although our inter-video fusion module is capable of integrating several paired of local features from the original video and the global features of the shuffled

video, it neglects the temporal information among the adjacent video frames. In this regard, we develop an intra-video fusion module to capture the temporal feature among adjacent video frames. Figure 3(c) shows the details of our intra-video fusion module, which further integrates three output features (P_{k-1}, P_k, and P_{k+1}) of inter-video fusion from three adjacent video frames. Let $P_k = (P_k^1, P_k^2, P_k^3)$, $P_{k-1} = (P_{k-1}^1, P_{k-1}^2, P_{k-1}^3)$, and $P_{k+1} = (P_{k+1}^1, P_{k+1}^2, P_{k+1}^3)$ to denote three CNN features of P_{k-1}, P_k, and P_{k+1}. To do so, our intra-video fusion module utilizes three attention blocks to integrate different CNN features, and i-th attention block fuses P_{k-1}^i, P_k^i, and P_{k+1}^i. Specifically, Figure 3(d) shows the schematic illustration of the i-th attention block. We first apply two linear layer on two input features P_k^i ($c \times w \times h$), and P_{k+1}^i ($c \times w \times h$), and then reshape both of them to two matrices, and their sizes are ($c \times wh$) and ($wh \times c$). We then multiply these two reshaped matrices to obtain a $wh \times wh$ similarity matrix, which is passed into a Softmax layer to fuse two input features P_k^i and P_{k+1}^i . Meanwhile, we utilize a linear layer on another input feature P_{k-1}^i ($c \times w \times h$) and reshape it into $c \times wh$. To further fuse P_{k-1}^i, we multiply its reshaped matrix with the similarity matrix from P_k^i and P_{k+1}^i to obtain a new feature ($c \times wh$), which is then reshaped into a 3D feature map ($c \times w \times h$); see Q_k^i of Figure 3(d). Mathematically, Q_k^i is computed by:

$$Q_k^i = \mathcal{R}(\hat{P}_{k-1}^i) \times Softmax\left(\mathcal{R}(\hat{P}_k^i) \times \mathcal{R}(\hat{P}_{k+1}^i) \right) \ , \tag{2}$$

where $\mathcal{R}$ denotes a reshape operation. $\hat{P}_k^i$, $\hat{P}_{k+1}^i$, and $\hat{P}_{k-1}^i$ represent the obtained features via utilizing a linear layer on three input features P_k^i, P_{k-1}^i, and P_{k+1}^i.

2.3 Our Network

Apparent from learning clip-level features (i.e., $P_k = (P_k^1, P_k^2, P_k^3)$) via fusing local and global temporal features via our inter-video fusion modules and our intra-video fusion module, we further learn a video-level information, which represents the classification result (benign or maligant) on each breast lesion of the input ultrasound video. To do so, we first pass three features (i.e., P_k^1, P_k^2, and P_k^3) of P_k into a multi-scale transformer (i.e., deformable-DETR [25]) to learn a long-range dependency feature map Z. We then apply a linear layer on Z to classify the breast lesions as benign lesions or malignant lesions. Furthermore, we predict bounding boxes of breast lesion as the final breast lesion detection result of the current video frame I_k (see Fig. 2). We utilize a negative log-likelihood to compute the lesion classification loss, and a linear combination of the ℓ_1 loss and the generalized IoU loss [12] for computing the breast lesion detection loss.

Implementation Details. We utilize ResNet-50 [5] pre-trained on ImageNet [3] to initialize the backbone of our network, and deformable DETR [25] pre-trained on COCO 2017 [8] to initialize the multi-scale transformer module of our network, while other network parameters are initialized by a normal distribution. All training videos are randomly horizontally flipped, resized, and cropped for data augmentation. Our network is implemented on Pytorch and trained using

Table 1. Quantitative comparisons of our network and compared methods on our annotated video dataset.

Method	Type	Backbone	AP	AP_{50}	AP_{75}
GFL [6]	image	ResNet-50	23.4	46.3	22.2
Cascade RPN [14]	image	ResNet-50	24.8	42.4	27.3
Faster R-CNN [11]	image	ResNet-50	25.2	49.2	22.3
VFNet [22]	image	ResNet-50	28.0	47.1	31.0
RetinaNet [7]	image	ResNet-50	29.5	50.4	32.4
DFF [26]	video	ResNet-50	25.8	48.5	25.1
FGFA [24]	video	ResNet-50	26.1	49.7	27.0
SELSA [17]	video	ResNet-50	26.4	45.6	29.6
Temporal ROI Align [4]	video	ResNet-50	29.0	49.9	33.1
MEGA [2]	video	ResNet-50	32.3	57.2	35.7
CVA-Net (ours)	video	ResNet-50	**36.1**	**65.1**	**38.5**

an Adam with 50 epochs, an initial learning rate of 2×10^{-4}, and a weight decay of 1×10^{-4}. The whole architecture is trained on three GeForce RTX 2080 Ti GPUs, and each GPU has a batch-size of 1.

3 Experiments and Results

Dataset. Note that there is no public ultrasound video breast lesion detection benchmark dataset with annotations. To evaluate the effectiveness of the developed network, we collect a breast lesion ultrasound video dataset with 188 videos, which has 113 malignant videos and 75 benign videos. These 118 videos has $25,272$ images in total, and the number of ultrasound images at each video varied from 28 to 413. Each video has a complete scan of the tumor, from its appearance to the largest section, then to its disappearance. All videos are acquired by LOGIQ-E9 and PHILIPS TIS L9-3. Two pathologists with eight years of experience in breast pathology were invited to manually annotate the breast lesion rectangles inside of each video frame and give the corresponding classification label for the breast lesions of the video. We further randomly and evenly select 38 videos from the dataset as a testing set (about 20% of the dataset) and the remaining videos as the training set.

Evaluation Metrics. We utilize three widely-used metrics for quantitatively comparing different ultrasound video breast lesion detection methods. They are average precision (AP), AP_{50}, and AP_{75}. Please refer to [15] for the definitions of AP, AP_{50}, and AP_{75}.

3.1 Comparisons with State-of-the-arts

We compare our network against ten state-of-the-art methods, including five image-based methods and five video-based methods. The image-based methods include, GFL [6], Cascade RPN [14], Faster R-CNN [11], VFNet [22], and RetinaNet [7]. The five video-based methods are DFF [26], FGFA [24], SELSA [17],
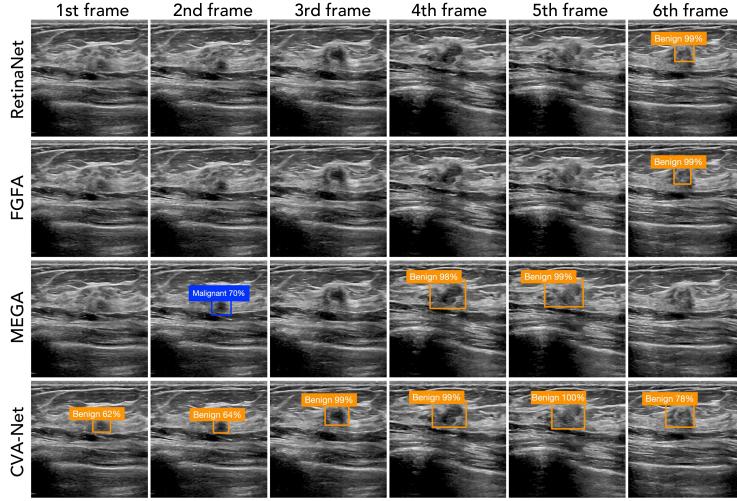
Fig. 4. Visual comparisons of video breast lesion detection results produced by our network and state-of-the-art methods (i.e., RetinaNet, FGFA, and MEGA) for multiple frames of an ultrasound video with benign breast lesions.

Temporal ROI Align [4], and MEGA [2]. For providing a fair comparison, we obtain the detection results of all compared methods by exploiting its public implementations or implementing them by ourselves. We also re-train these networks on our dataset, and fine-tune the network parameters for achieving the best detection results of ultrasound video breast lesions.

Quantitative Comparisons. Table 1 summarizes the quantitative results of our network and all ten compared breast lesion video detection methods. In general, video-based methods tend to have larger AP, AP_{50}, and AP_{75} scores than image-based ones. Specifically, among ten compared methods, MEGA has the largest AP score of 32.3, the largest AP_{50} score of 57.2, and the largest AP_{75} score of 35.7. On the contrary, our method further outperforms MEGA in terms of all three metrics (AP, AP_{50}, and AP_{75}). Compared to MEGA, our CVA-Net improves the AP score from 32.3 to 36.1, the AP_{50} score from 57.2 to 65.1, and the AP_{75} score from 35.7 to 38.5.

Visual Comparisons. Fig. 4 visually compares breast lesion detection results produced by our network and four compared methods for multiple frames of an ultrasound video with benign breast lesions. As shown in the first two rows of Figure 4, RetinaNet and FGFA fail to detect the breast lesions of the first five frames. MEGA obtains a better breast lesion detection result among three compared methods, but also fails to detect breast lesions at the 1st, 3rd, and 6th video frames. Moreover, although MEGA can detect the breast lesion of the 2nd frame, the classification result is incorrect (see the blue rectangle of Fig. 4). However, our method (see CVA-Net at last row of Fig. 4) can correctly detect the breast lesions of all video frames and has a correct breast lesion classification result for each video frame.

Table 2. Quantitative results of ablation study experiments. "Ours-w/o-cla" is to remove the lesion classification branch from our network. "Ours-w/o-aug" denotes that we do not utilize any data augmentation operation on shuffled video frames, while "Ours-VF", "Ours-RR", and "Ours-CC" denote that we utilize the vertical flip, random rotation, and center crop operation on the shuffled video frames.

	AP	AP_{50}	AP_{75}
Basic	27.8	52.8	26.4
Basic+Inter-video	33.5	55.1	38.5
Basic+Intra-video	27.8	60.9	36.3
Our method	**36.1**	**65.1**	**38.5**
Ours-w/o-cla	34.4	61.4	35.5
Ours-w/o-aug	35.6	62.1	37.8
Ours-VF	35.5	59.8	37.1
Ours-RR	35.4	62.1	38.4
Ours-CC	35.8	62.4	37.9

3.2   Ablation Study

Effectiveness of clip-level features. We first construct three baselines to verify the clip-level features learned by our inter-video fusion and intra-video fusion. The first baseline network ("basic") is to remove all inter-frame fusion modules and the intra-frame fusion modules from our network. The second baseline network ("basic+inter-video") is to add inter-video fusion module into "basic", while the third one ("basic+intra-video") is to add the intra-video fusion module into "basic". As shown in Table 2, "basic+inter-video" has a larger AP, AP_{50}, and AP_{75} scores than "basic", showing that the leveraging our inter-video fusion module to fuse local information of the input video and global information of the shuffled video can enhance the breast lesion detection performance in ultrasound video. Moreover, our network achieves superior results of AP, AP_{50}, and AP_{75} over "basic+inter-video" and "basic+intra-video". It improves the AP score from 27.8 to 36.1, the AP_{50} score from 52.8 to 65.1, and the AP_{75} score from 26.5 to 38.6. It indicates that integrating the inter-video fusion module and the intra-video fusion module together in our method can further enhance the breast lesion detection accuracy in ultrasound video.

Effectiveness of video-level features. We also compare our method with and without the lesion classification branch and show their results in Table 2. It shows that the video breast lesion detection accuracy of our method are reduced when we remove the lesion classification branch from our network.

Effectiveness of data augmentation on shuffled video frames. Note that we have utilized a data augmentation technique (i.e., random pepper) on shuffled video frames before passing them into the feature extraction backbone (see Encoder of Fig. 2). Hence, we further show the video breast lesion detection results of our network without and with different data augmentation techniques, including vertical flip, random rotation, and center crop. Apparently, our method

with a random pepper has the best detection performance, and thus our network empirically utilizes this data augmentation in our experiments.

4   Conclusion

This paper first collects and annotates the first ultrasound video dataset for breast lesion detection with 188 videos. Moreover, we present a clip-level and video-level feature aggregation network for boosting breast lesion detection in ultrasound videos. The main idea of our network is to combine clip-level features and video-level features for detecting breast lesions in videos, and the clip-level features are learned by devising inter-video fusion modules and intra-video fusion on the input ordered video and a shuffled video. Experimental results on our annotated dataset show that our network has obtained superior breast lesion detection performance over state-of-the-art methods. Our further work includes the collection of more video data, exploration of a more systematic approach or complicated video shuffling operations.

References

1. Chen, S., Yu, W., Ma, K., Sun, X., Lin, X., Sun, D., Zheng, Y.: Semi-supervised breast lesion detection in ultrasound video based on temporal coherence. arXiv preprint arXiv:1907.06941 (2019)
2. Chen, Y., Cao, Y., Hu, H., Wang, L.: Memory enhanced global-local aggregation for video object detection. In: Proceedings of the IEEE/CVF Conference on Computer Vision and Pattern Recognition. pp. 10337–10346 (2020)
3. Deng, J., Dong, W., Socher, R., Li, L.J., Li, F.F.: Imagenet: A large-scale hierarchical image database. In: IEEE Conference on Computer Vision and Pattern Recognition (2009)
4. Gong, T., Chen, K., Wang, X., Chu, Q., Zhu, F., Lin, D., Yu, N., Feng, H.: Temporal roi align for video object recognition. In: Proceedings of the AAAI Conference on Artificial Intelligence. vol. 35, pp. 1442–1450 (2021)
5. He, K., Zhang, X., Ren, S., Sun, J.: Deep residual learning for image recognition. IEEE Conference on Computer Vision and Pattern Recognition (CVPR) pp. 770–778 (2016)
6. Li, X., Wang, W., Wu, L., Chen, S., Hu, X., Li, J., Tang, J., Yang, J.: Generalized focal loss: Learning qualified and distributed bounding boxes for dense object detection. arXiv preprint arXiv:2006.04388 (2020)
7. Lin, T.Y., Goyal, P., Girshick, R., He, K., Dollár, P.: Focal loss for dense object detection. In: Proceedings of the IEEE International Conference on Computer Vision. pp. 2980–2988 (2017)

8. Lin, T.Y., Maire, M., Belongie, S., Hays, J., Perona, P., Ramanan, D., Dollár, P., Zitnick, C.L.: Microsoft coco: Common objects in context. In: European Conference on Computer Vision. pp. 740–755. Springer (2014)

9. Movahedi, M.M., Zamani, A., Parsaei, H., Tavakoli Golpaygani, A., Haghighi Poya, M.R.: Automated analysis of ultrasound videos for detection of breast lesions. Middle East Journal of Cancer **11**(1), 80–90 (2020)

10. Qi, X., Zhang, L., Chen, Y., Pi, Y., Chen, Y., Lv, Q., Yi, Z.: Automated diagnosis of breast ultrasonography images using deep neural networks. Medical image analysis **52**, 185–198 (2019)

11. Ren, S., He, K., Girshick, R., Sun, J.: Faster r-cnn: Towards real-time object detection with region proposal networks. arXiv preprint arXiv:1506.01497 (2015)

12. Rezatofighi, S.H., Tsoi, N., Gwak, J., Sadeghian, A., Reid, I., Savarese, S.: Generalized intersection over union: A metric and a loss for bounding box regression. IEEE/CVF Conference on Computer Vision and Pattern Recognition (CVPR) pp. 658–666 (2019)

13. Stavros, A.T., Thickman, D., Rapp, C.L., Dennis, M.A., Parker, S.H., Sisney, G.A.: Solid breast nodules: use of sonography to distinguish between benign and malignant lesions. Radiology **196**(1), 123–134 (1995)

14. Vu, T., Jang, H., Pham, T.X., Yoo, C.D.: Cascade rpn: Delving into high-quality region proposal network with adaptive convolution. ArXiv **abs/1909.06720** (2019)

15. Wang, X., Kong, T., Shen, C., Jiang, Y., Li, L.: Solo: Segmenting objects by locations. In: European Conference on Computer Vision. pp. 649–665. Springer (2020)

16. Wild, C., Weiderpass, E., Stewart, B.W.: World cancer report: cancer research for cancer prevention. IARC Press (2020)

17. Wu, H., Chen, Y., Wang, N., Zhang, Z.: Sequence level semantics aggregation for video object detection. 2019 IEEE/CVF International Conference on Computer Vision (ICCV) pp. 9216–9224 (2019)

18. Xue, C., Zhu, L., Fu, H., Hu, X., Li, X., Zhang, H., Heng, P.A.: Global guidance network for breast lesion segmentation in ultrasound images. Medical Image Analysis p. 101989 (2021)

19. Yang, Z., Gong, X., Guo, Y., Liu, W.: A temporal sequence dual-branch network for classifying hybrid ultrasound data of breast cancer. IEEE Access **8**, 82688–82699 (2020)

20. Yap, M.H., Pons, G., Marti, J., Ganau, S., Sentis, M., Zwiggelaar, R., Davison, A.K., Marti, R.: Automated breast ultrasound lesions detection using convolutional neural networks. IEEE journal of biomedical and health informatics **22**(4), 1218–1226 (2017)

21. Zhang, E., Seiler, S., Chen, M., Lu, W., Gu, X.: Birads features-oriented semi-supervised deep learning for breast ultrasound computer-aided diagnosis. Physics in Medicine & Biology **65**(12), 125005 (2020)

22. Zhang, H., Wang, Y., Dayoub, F., Sunderhauf, N.: Varifocalnet: An iou-aware dense object detector. IEEE/CVF Conference on Computer Vision and Pattern Recognition (CVPR) pp. 8510–8519 (2021)

23. Zhu, L., Chen, R., Fu, H., Xie, C., Wang, L., Wan, L., Heng, P.A.: A second-order subregion pooling network for breast lesion segmentation in ultrasound. In: International Conference on Medical Image Computing and Computer-Assisted Intervention. pp. 160–170. Springer (2020)

24. Zhu, X., Wang, Y., Dai, J., Yuan, L., Wei, Y.: Flow-guided feature aggregation for video object detection. IEEE International Conference on Computer Vision (ICCV) pp. 408–417 (2017)

25. Zhu, X., Su, W., Lu, L., Li, B., Wang, X., Dai, J.: Deformable detr: Deformable transformers for end-to-end object detection. arXiv preprint arXiv:2010.04159 (2020)
26. Zhu, X., Xiong, Y., Dai, J., Yuan, L., Wei, Y.: Deep feature flow for video recognition. In: Proceedings of the IEEE Conference on Computer Vision and Pattern Recognition. pp. 2349–2358 (2017)